Journal of The Electrochemical Society, **148** (1) A24-A29 (2001)
S0013-4651/2001/148(1)/A24/6/$7.00 © The Electrochemical Society, Inc.

The Role of Carbon Black in $LiMn_2O_4$-Based Composites as Cathodes for Rechargeable Lithium Batteries

Sankar Mandal,[a] J. Manuel Amarilla,[a] J. Ibáñez,[b] and José M. Rojo[a,z]

[a]*Instituto Ciencia de Materiales de Madrid, Consejo Superior de Investigaciones Cientificas, Cantoblanco, 28049 Madrid, Spain*
[b]*Centro Nacional de Investigaciones Metalúrgicas, Consejo Superior de Investigaciones Cientìficas, 28040 Madrid, Spain*

$LiMn_2O_4$-based composites have been prepared by cold pressing physical mixtures of $LiMn_2O_4$, carbon black (CB), and polyvinylidenefluoride (PVDF). The PVDF content has been kept constant (*ca.* 14.5% by volume or 10% by weight). The $LiMn_2O_4$ and CB contents have been changed in an opposite way, *i.e.*, from 59.6 vol % (or 90.6 wt %) to 19.2 vol % (or 49 wt %) for $LiMn_2O_4$, and from 0 vol % (or 0 wt %) to 32.2 vol % (or 38 wt %) for CB. The microstructure of the composites shows clusters formed of aggregated particles of either $LiMn_2O_4$ or CB. The electrical conductivity follows a percolating process in which the conductivity changes by five orders of magnitude, the percolation threshold being 3 vol % of CB. The first discharge capacity changes from 0 to 135 $mAhg^{-1}$ for increasing the CB content. The change in capacity also seems to follow a percolation process in which the sharp increase in capacity is observed for CB contents close to 3 vol %. The discharge capacity of the $LiMn_2O_4$-based composites is controlled by electronic transport within the composite, the electronic transport depending on the microstructure of the composite.
© 2000 The Electrochemical Society. S0013-4651(00)06-068-7. All rights reserved.

Manuscript submitted June 19, 2000; revised manuscript received June 27, 2000.

In the last two decades cathodic materials for rechargeable lithium batteries have been extensively studied because these batteries show elevated potential, high energy density, long shelf-life, and safety.[1,2] Among the cathodic materials investigated $LiMn_2O_4$-based spinels are promising candidates to replace $LiCoO_2$, which is the material currently used in commercial lithium batteries. In fact, the low cost of the manganese compounds together with their acceptable environmental requirement make these compounds suitable for cathodic materials.[3-15]

It is worth noting that the positive electrodes (cathodes) of the lithium batteries are normally composites in which, besides the active electrode material ($LiCoO_2$, $LiMn_2O_4$, etc.), a polymer and a good electronic conductor are usually added. So, it seems that a detailed knowledge of the composites is needed for improving their electrochemical response as positive electrodes. Carbon black (CB) is generally chosen because of its good electronic conductivity which assures an efficient electronic transport through the composite. The efficiency in electronic transport is required because the deinsertion/insertion of Li^+ ions in the active material is accompanied by oxidation/reduction of some of its elements (Mn, Co, etc.). Moreover, it seems that CB favors a good absorption of the liquid electrolyte by the composite, and hence, a good contact between Li^+ ions and the particles of the active material. The polymer, which is normally an insulating material from the electrical point of view, can be used as a binder for improving handling of the composite.[1,2] In binary composites formed of a polymer and a good electronic conductor such as CB, graphite, etc., the relative content of the components and, specially, their distribution within the composite are responsible for the electrical conductivity found.[16-22] In ternary composites formed of $LiMn_2O_4$, CB, and a polymer, the relative content of the three compounds would be the parameter more strongly affecting the electrical conductivity as well as the electrochemical response of the composites. However, this point has not been analyzed in detail so far.

In this work we have prepared composites from physical mixtures of $LiMn_2O_4$, CB, and polyvinylidenefluoride (PVDF). The content in PVDF was kept constant, and we analyzed how the electrical conductivity and the discharge capacity were changed as a function of the relative content in $LiMn_2O_4$ and CB. The significant variation found in both conductivity and capacity is discussed in terms of the microstructure of the composites as followed by scanning electron microscopy (SEM).

[z] E-mail: jmrojo@icmm.csic.es

Experimental

Composites of different composition were prepared by mixing and grinding the three components, $LiMn_2O_4$, polyvinylidenefluoride (PVDF), and carbon black (CB), in an agate mortar. Cylindrical and parallelepiped pellets of the composites as well as of the individual components were obtained by cold pressing at 170 MPa in conventional equipment. The dimensions of the pellets were 13 mm in diameter and *ca*. 1 mm in height for the pellets with cylindrical shape, and 10 × 3 mm surface and *ca*. 3 mm in height for those of parallelepiped shape. The force was applied in the direction perpendicular to the pellet surface. The cylindrical pellets were used for the electrochemical experiments. Both cylindrical and parallelepiped pellets were used for determining the electrical conductivity and analyzing the microstructure of the composite. $LiMn_2O_4$ was obtained from the solid-state reaction of Mn_2O_3 and $LiNO_3$ following the procedure described elsewhere.[23] The cubic cell parameter of $LiMn_2O_4$ was 8.2418(9) Å, and its Brunauer-Emmett-Teller (BET) surface area was 7.5 m^2/g^{-1}. PVDF (Mw ≈ 534,000) and CB (Super P carbon black) were commercial products supplied by Fluka and MMM Carbon, respectively. The BET surface area of CB was 60.7 m^2/g^{-1}. The density, determined by helium adsorption, was 1.80 g cm^{-3} for PVDF and 1.98 g cm^{-3} for CB. The calculated crystallographic density for $LiMn_2O_4$ was 4.28 g cm^{-3}.

Two- or four-probe impedance measurements were carried out in a 1260 Solartron impedance/gain phase analyzer at room temperature. These measurements were done on pellets of the composites in the frequency range 5-10^6 Hz. Silver paint was used as the electrode.

SEMs were obtained in a JEOL 200 microscope coupled to an energy dispersive spectrometer (EDS). Transmission electron micrographs (TEMs) were obtained in a JEOL 2000 EX microscope. Pellets of the composites were mounted in resin and examined by SEM in the same direction in which the alternating electric field was applied during the impedance measurements.

The electrochemical characterization of the $LiMn_2O_4$-based composites was carried out in a lithium cell. The cathodic composites contained between 100 and 140 mg of $LiMn_2O_4$. The electrolyte was a 1 M solution of $LiPF_6$ in anhydrous ethylene carbonate and dimethyl carbonate in a 1:1 weight ratio. The negative electrode (anode) was a lithium foil, which also operated as the reference electrode. The different components were placed in a Swagelock™ cell, and were assembled in an argon glove box in which the water content was below 1 ppm. The cells were galvanostatically cycled in an Arbin instrument (model BT 2043) between 3.3 and 4.5 V at a con-

Ningde Amperex Tech. Exhibit No. 2039
Zhuhai CosMX Battery Co. Ltd. v. Ningde Amperex Tech.
IPR2025-00431, U.S. Patent No. 11,799,131
Page 1 of 6

stant current of C/24, C/12, and C/5. C is the capacity of the cathode calculated from the theoretical capacity of $LiMn_2O_4$ (C = 148 mAh) and the mass of this compound in the composite. The values 24, 12, and 5 are the experimental times expressed in hours.

Results and Discussion

The PVDF powder as examined by SEM is shown in Fig. 1a. The particles show a granular texture with sizes in the range 2-8 μm. The $LiMn_2O_4$ powder as examined by TEM is shown in Fig. 1b. The shape of the particles is irregularly faceted; the sizes being in the range of 0.1-0.4 μm. The TEM photograph for CB powder is shown in Fig. 1c. These particles are platelets with sizes in the range of 0.01-0.05 μm. The particle size is quite different for the powders of the three compounds; the particle size decreases by *ca*. ten times from PVDF to $LiMn_2O_4$, and by *ca*. ten times from $LiMn_2O_4$ to CB.

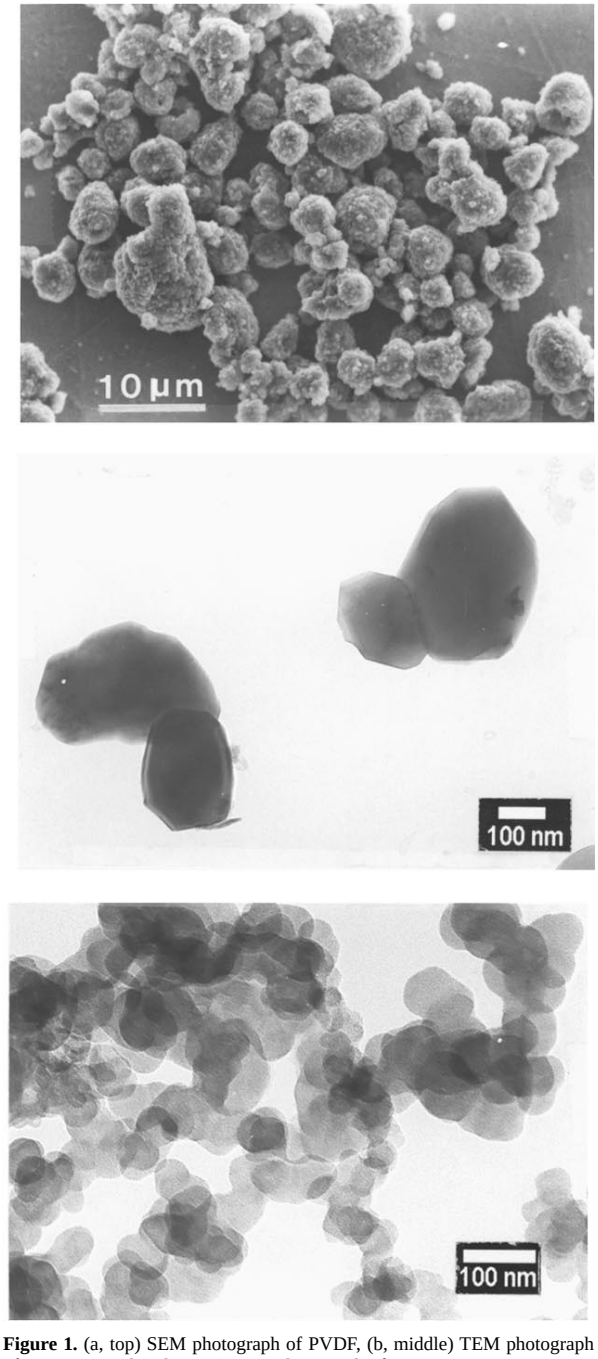

Figure 1. (a, top) SEM photograph of PVDF, (b, middle) TEM photograph of $LiMn_2O_4$, and (c, bottom) TEM photograph of CB.

Table I. Volume content in PVDF, $LiMn_2O_4$, CB, and air of pellets prepared by cold pressing at 170 MPa of the PVDF, $LiMn_2O_4$, and CB powders.

Pellet (nominal)	Compound (vol %)	Air (vol %)
PVDF	90	10
$LiMn_2O_4$	62	38
CB	15	85

Pellets of each individual component (PVDF, $LiMn_2O_4$, and CB) were prepared and the volume content of each compound was determined from its mass and density. The remaining volume up to the pellet volume was assumed to be air. The volume contents of each compound and of air for the three pellets are outlined in Table I. The air content is only 10 vol % for the PVDF pellet, it is as high as 85 vol % for the CB pellet. Therefore the PVDF pellet is much more compacted than the CB one. Compaction of the $LiMn_2O_4$ pellet is intermediate between the other two pellets.

Composites.—The composites prepared in this work from a physical mixture of the three materials (PVDF, $LiMn_2O_4$, and CB) are outlined in Table II. The weight content of PVDF was close to 10% for all the composites. The weight contents of $LiMn_2O_4$ and CB changed in an opposite way. The volume content of each component was determined from their mass and density as already mentioned. The volume content in air, which gives a measurement of the porosity of the pellets, is also included in the Table II. The composites are labeled as COM followed by the CB volume content in percent. It is observed that the air volume content for the COM-0 composite (25.6 vol %) is lower than that for the pellet of $LiMn_2O_4$ alone (38 vol %), and the air volume content for the COM-32.2 (36.4 vol %) is also lower than that for the pellet of CB alone (85 vol %). So, it seems that the presence of PVDF decreases the air content and favors compaction of the pellets.

The variation (in volume) of $LiMn_2O_4$, air, and PVDF *vs*. CB is shown in Fig. 2. The PVDF content is practically constant as established in the study. The $LiMn_2O_4$ content decreases for increasing the CB content as a consequence that the second compound replaces the first one. The increase in air with the increase in CB points out that air is mainly associated with CB. This interpretation is also in agreement with the higher air content found for the pellet of CB alone compared with the pellets of $LiMn_2O_4$ and PVDF (see Table I).

Electrical conductivity.—The impedance plots recorded at room temperature for the COM-1.5 and COM-6.4 composite are shown in Fig. 3. A depressed arc is observed for the first composite. The resistance, deduced from the intercept of the arc with the real Z' axis, is $1.2 \times 10^4\ \Omega$. The conductivity of the pellet, calculated from the resistance measured and the cell constant, is 4.8×10^{-5} S cm^{-1}. The capacitance of the arc, deduced from the ideal equation $\omega RC = 1$, is 32 pF; where ω is the angular frequency at the maximum of the arc, R is the resistance, and C is the capacitance. The value of the conductivity is close to that found for a pellet of $LiMn_2O_4$ alone.[24-28] This indicates that the electrical conductivity of COM-1.5 is dominated by $LiMn_2O_4$, which is an n-type semiconductor. The high capacitance found compared with that usually reported for the bulk (or grain interior) response (1-10 pF)[29,30] indicates that grain boundaries are also involved in that arc. The impedance plot for the COM-6.4 composite shows only one point whose resistance is 30 Ω. The conductivity calculated for the pellet of this composite is 1.2×10^{-1} S cm^{-1}. As this value is close to that found for the pellet of CB alone (1.5×10^{-1} S cm^{-1}), we can conclude that CB dominates the electrical conductivity of the COM-6.4 composite. CB is also an n-type semiconductor, but the capacitance

Ningde Amperex Tech. Exhibit No. 2039
Zhuhai CosMX Battery Co. Ltd. v. Ningde Amperex Tech.
IPR2025-00431, U.S. Patent No. 11,799,131
Page 2 of 6

Table II. Weight (wt) and volume (vol) contents of PVDF, $LiMn_2O_4$, and CB for the composites prepared. The air volume content is also included. The composites are labeled as COM followed by the CB volume content.

Composite	PVDF		$LiMn_2O_4$		CB		Air
	wt (%)	vol (%)	wt (%)	vol (%)	wt (%)	vol (%)	vol (%)
COM-0	9.4	14.8	90.6	59.6	0	0	25.6
COM-1.5	9.5	14.6	89.4	57.7	1.1	1.5	26.1
COM-2.1	9.5	14.6	89	57.2	1.5	2.1	26.1
COM-2.8	9.5	14.5	88.5	56.6	2	2.8	26.1
COM-3.7	9.6	14.7	87.7	56.1	2.7	3.7	25.5
COM-4.4	9.7	14.8	87.1	55.7	3.2	4.4	25
COM-5	9.8	14.7	86.5	54.3	3.7	5	25.9
COM-6.4	10	14.7	85.2	52.4	4.8	6.4	26.5
COM-7.9	10	14.6	84	51.3	6	7.9	26.2
COM-10.7	10	13.9	81.5	47.3	8.5	10.7	28
COM-11.9	10.5	14.1	79.7	44.9	9.8	11.9	29
COM-14.7	11	14.1	78	47.9	11	14.7	23.3
COM-19.4	11	13.8	72	37.8	17	19.4	29
COM-23.9	11	11.5	64	28.1	25	23.9	36.5
COM-29.6	12.5	13.1	56.5	24.8	31	29.6	32.4
COM-32.2	12	13	49	19.2	38	32.2	36.5

contribution is not observed at room temperature; this contribution, however, could be observed at lower temperatures. Therefore the electrical conductivity, which is of the electronic type, is dominated either by $LiMn_2O_4$ or by CB depending on their relative contents.

The variation of the electrical conductivity *vs.* CB volume fraction is shown in Fig. 4. A sharp increase in conductivity is observed for low CB volume fractions. The conductivity increases slightly for higher contents, and for CB volume fractions above 0.15 the conductivity is almost constant. The experimental data are well fitted to a percolation equation $\sigma = \sigma_0(v - v_c)^t$, for $v \geq v_c$; where v is the CB volume fraction, v_c is the CB volume fraction at the percolation threshold, t is the exponent, and σ_0 is a pre-exponential factor.[31,32] From this fitting we have deduced that $v_c = 0.03$, *i.e.*, 3 vol % that corresponds to 2.0 wt %. Therefore, while for CB volume fractions below 0.03 the electrical conductivity of the composite is mainly due to $LiMn_2O_4$, for CB contents above 0.03 CB dominates the electrical conductivity. It suggests

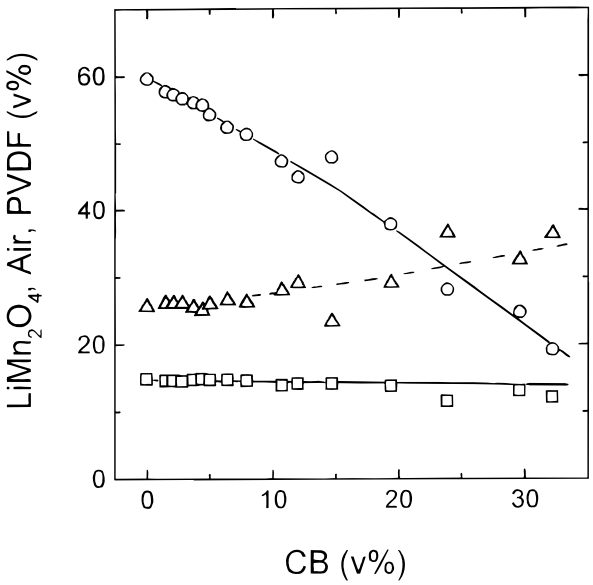

Figure 2. Variation in volume of $LiMn_2O_4$ (circles), air (triangles), and PVDF (squares) as a function of CB volume content. The lines are marked to guide the eye.

that while the $LiMn_2O_4$ particles are connected along the composite below the percolation threshold, the CB particles are connected above the percolation threshold. The contributions of PVDF and air to the composite conductivity are negligible because they are insulators. The low volume fraction found ($v_c = 0.03$) compared with that predicted for a random distribution of particles ($v_c = 0.15$-0.17) suggests to us that the CB particles are easily connected along the composite.

Microstructure.—To ascertain how the three components, $LiMn_2O_4$, CB, and PVDF, are distributed within the composites, some composites were analyzed by SEM. The micrographs obtained for the COM-1.5, COM-6.4, and COM–32.2 composite are shown in Fig. 5a, b, and c, respectively. From microanalysis data the white areas were identified as $LiMn_2O_4$. The size of these areas is larger than the size of the $LiMn_2O_4$ particles as analyzed by TEM, and this fact points out that the white areas are clusters formed from the aggregation of $LiMn_2O_4$ particles. The contribution of the isolated $LiMn_2O_4$ particles to the SEM images is negligible because the area fraction of $LiMn_2O_4$ estimated from the images is coincident with the volume fraction of this compound in the composite. The size of the different $LiMn_2O_4$ clusters was estimated by using an image analysis program.

The histogram of the cluster size in a semi-log scale is shown in Fig. 6 (top). The percentage of $LiMn_2O_4$ clusters having sizes in the range 0.4-0.8 μm shows a maximum for the three composites. However, there are also a few $LiMn_2O_4$ clusters with sizes higher than 6.4 μm whose contribution to the area of the analyzed images is very important. In Fig. 6 (bottom) we have plotted the area *vs.* size for all the clusters found. For the COM-32.2 composite a maximum in area is observed for clusters with sizes in the range 6.4-12.8 μm. This maximum is shifted toward higher sizes (25.6-51.2 μm) for the COM-6.4 composite which is richer in $LiMn_2O_4$. For the COM-1.5 composite, with very high $LiMn_2O_4$ content, a bimodal distribution with two maxima is observed: one maximum at 25.6-51.2 μm, and the other at 204.8-409.6 μm. The second maximum is due to the presence of connected clusters of $LiMn_2O_4$ that are extended along the composite. The presence of this maximum is associated with the fact that $LiMn_2O_4$, as already mentioned, dominates the electrical conductivity of the COM-1.5 composite. The first maximum, which is also observed at the same size for the COM-6.4 composite and at lower size for the COM-32.2 composite, seems to be associated with clusters that remain unconnected in the composite. This interpretation is supported by the fact that $LiMn_2O_4$ does not dominate the electrical conductivity of the COM-6.4 and COM-32.2 composite; in both composites CB dominates their electrical conductivity.

The black areas in Fig. 5 were ascribed to PVDF, CB, and air, although we could not distinguish among them. As the sizes of the

Ningde Amperex Tech. Exhibit No. 2039
Zhuhai CosMX Battery Co. Ltd. v. Ningde Amperex Tech.
IPR2025-00431, U.S. Patent No. 11,799,131
Page 3 of 6

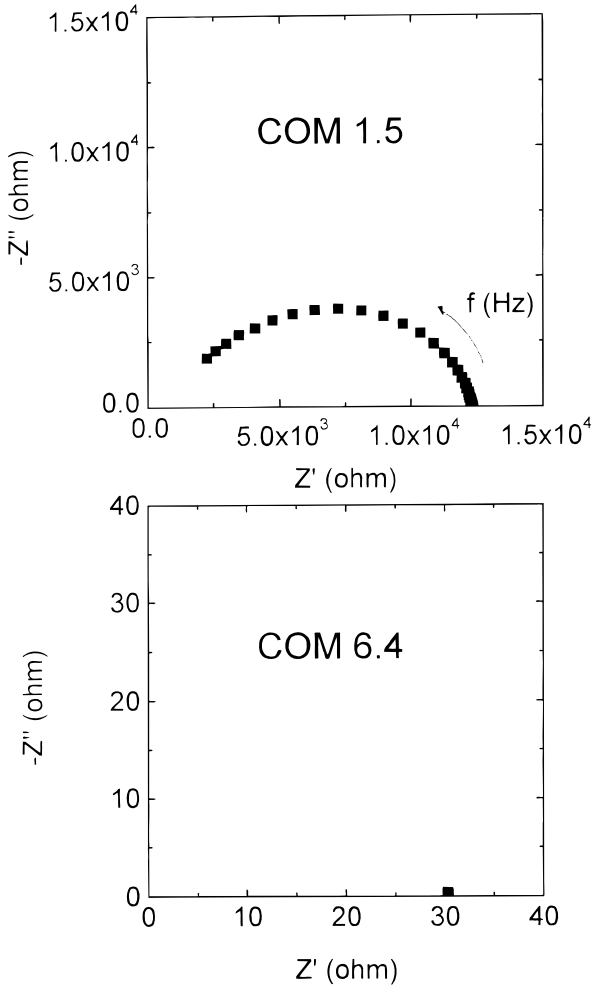

Figure 3. Impedance plots recorded at room temperature for the COM 1.5 and COM 6.4 composite.

black areas are also larger than the size of PVDF and CB particles, it seems that the black areas are also clusters of these compounds.

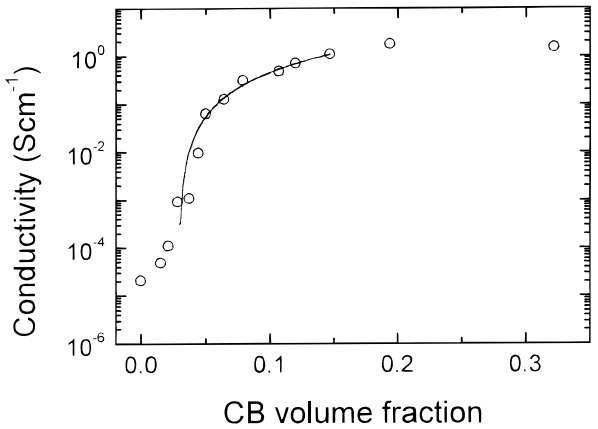

Figure 4. Electrical conductivity *vs.* carbon black volume fraction. The solid line stands for the best fit to the equation $\sigma = \sigma_0(v - v_c)^t$; the fitting parameters are $\sigma_0 = 41$ S cm^{-1}, $v_c = 0.03$, $t = 1.7$.

However, as the PVDF content is almost constant and the black areas become more important when the CB content increases, we can assume that the black areas are mainly due to CB clusters. This is in agreement with the fact that CB dominates the electrical conductivity of composites that show extended black areas (see, for example, the SEM image of the COM-32.2 composite in Fig. 5).

Discharge capacity.—The galvanostatic discharge curves for the COM-4.4 and COM-32.2 composite between the cutoff voltages

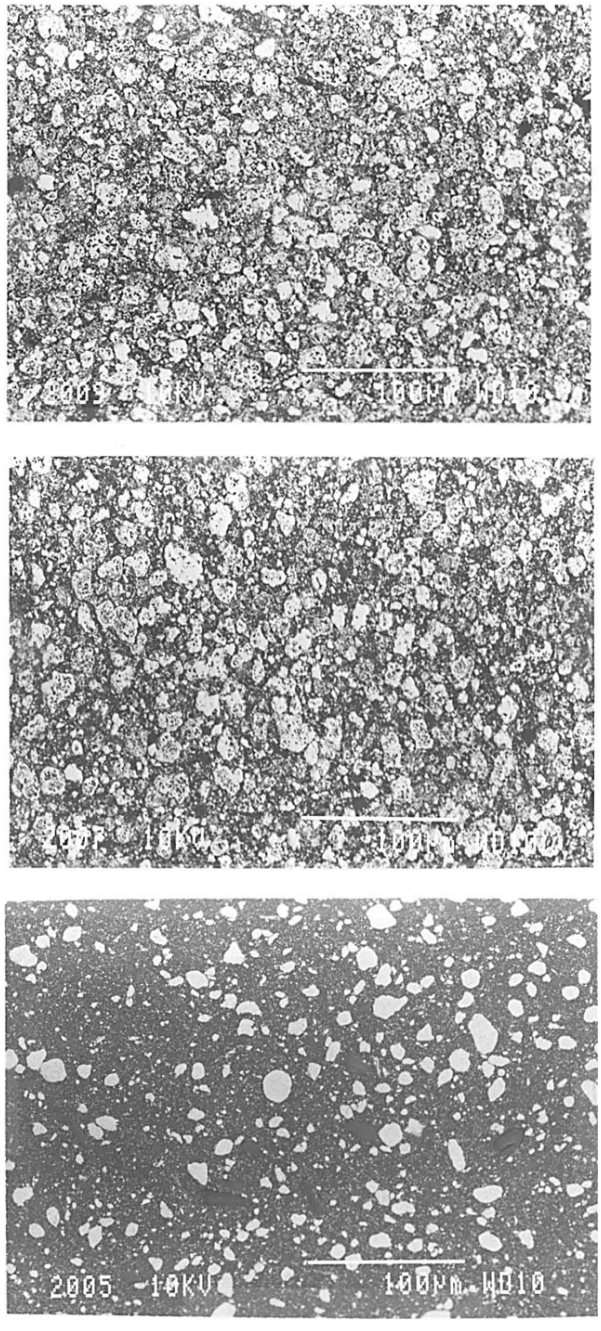

Figure 5. SEM photographs obtained for the (a, top) COM 1.5, (b, middle) COM 6.4, and (c, bottom) COM 32.2 composite. White areas were identified as $LiMn_2O_4$. Black areas were ascribed to CB, PVDF, and air.

Ningde Amperex Tech. Exhibit No. 2039
Zhuhai CosMX Battery Co. Ltd. v. Ningde Amperex Tech.
IPR2025-00431, U.S. Patent No. 11,799,131
Page 4 of 6

of 3.3 and 4.5 V are shown in Fig. 7. These curves correspond to the first discharge, and they were obtained under a C/24 current. The shape of these curves is similar, showing the typical two plateaus usually reported for $LiMn_2O_4$.[1-15] Nevertheless, the discharge capacity is different being higher for the COM-32.2 composite, *i.e.*, for the composite with higher CB content. We have also recorded galvanostatic curves at higher currents (C/12 and C/5) for the different composites (not shown), and we have determined their first discharge capacity.

The variation of the first discharge capacity *vs.* carbon black volume fraction is shown in Fig. 8. The $LiMn_2O_4$ volume fraction is also shown. We have included for comparison the capacities obtained when the galvanostatic experiments were made at the C/24, C/12, and C/5 current. For the three experiments the capacity is close to zero for the CB volume fractions below 0.03, *i.e.*, the composites did not show any electrochemical response. The capacity increases sharply for CB volume fractions close to 0.03, the increase being less important for the experiment made at the C/5 current. For higher CB volume fractions the capacity increases gradually up to a maximum value of 135 mAh g^{-1} for the experiments made at the C/24 and C/12 current, and up to a value of 122 mAh g^{-1} for the experiment made at C/5. Therefore, the discharge capacity of the composites increases on increasing the CB volume fraction despite the significant decrease in $LiMn_2O_4$ volume fraction from 0.58 to 0.19.

The decrease in capacity on increasing current is as usual. However, we find that the decrease is more important for the composites having CB contents close to the percolation threshold than for those having high CB contents. Thus, while the capacity of the COM-4.4

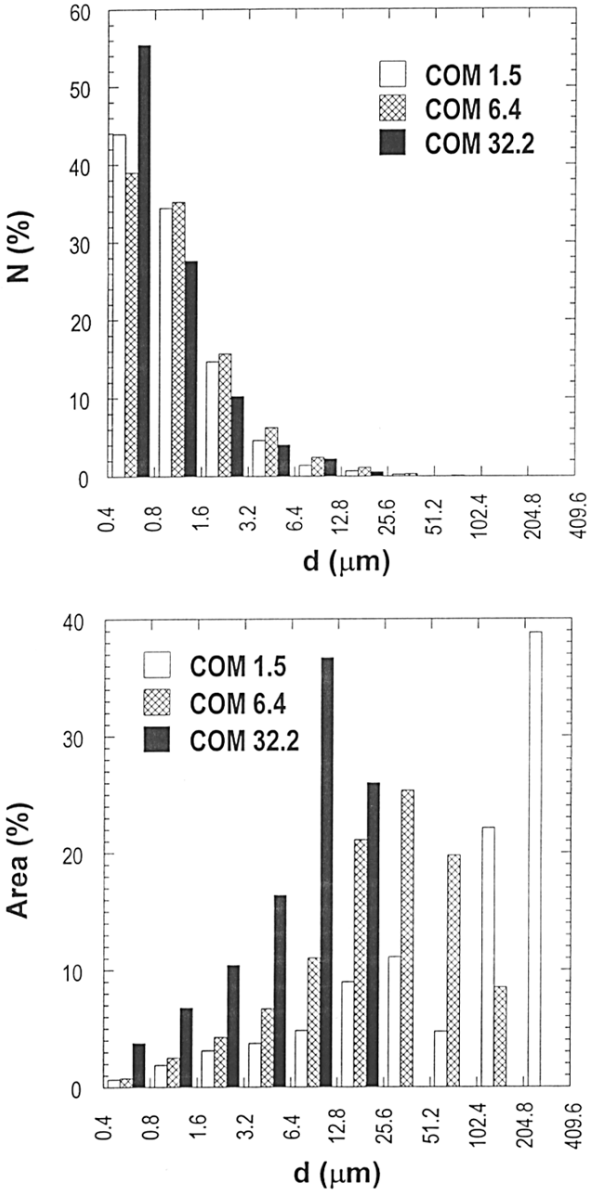

Figure 6. Top: size distribution histogram of $LiMn_2O_4$ clusters. Bottom: cluster area *vs.* cluster size. The white, shadow, and black bars stand for the COM 1.5, COM 6.4, and COM 32.2 composite, respectively.

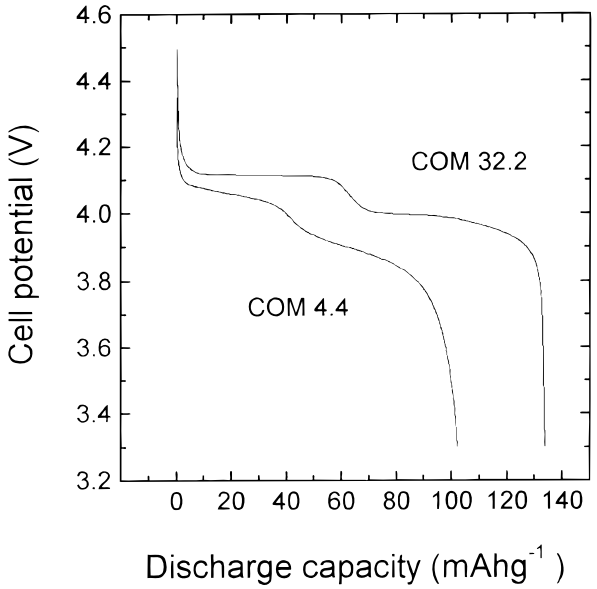

Figure 7. Galvanostatic curves obtained in the first discharge for the COM 4.4 and COM 32.2 composite. The current used was C/24.

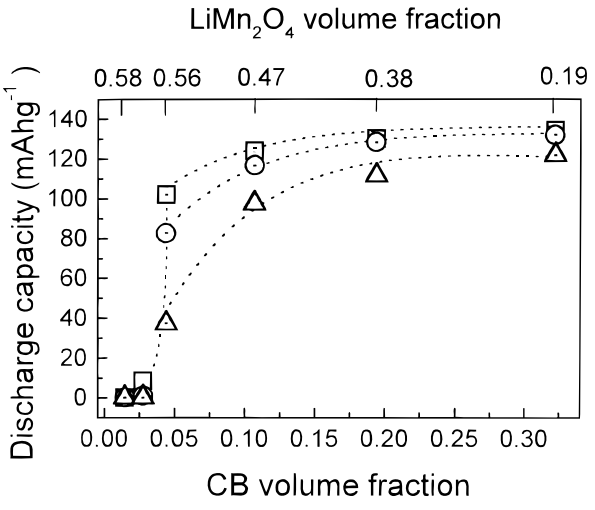

Figure 8. Variation of the first discharge capacity *vs.* carbon black volume fraction. Squares, circles, and triangles stand for the experiments made at the C/24, C/12, and C/5 current, respectively. The dashed lines are drawn to guide the eye.

Ningde Amperex Tech. Exhibit No. 2039
Zhuhai CosMX Battery Co. Ltd. v. Ningde Amperex Tech.
IPR2025-00431, U.S. Patent No. 11,799,131
Page 5 of 6

composite at the C/24 current decreases by 63% when the experiment is done at the C/5 current, the capacity of the COM-32.2 at the C/24 current only decreases by 9% when the experiment is done at the C/5 current. These results point out that the kinetic of the electrochemical reaction, due to lithium diffusion in the active material, is also affected or modulated by the microstructure of the composite.

We find that all the capacity curves (Fig. 8) are similar to the electrical conductivity curve (Fig. 4), and the sharp increase in both capacity and conductivity is observed at the same CB volume fraction. Based on these results we can establish that the electrical conductivity and the discharge capacity of the composite depend on the CB content in the same way, *i.e.*, according to a percolation process. The discharge capacity curves account for two processes that occur simultaneously in λ-MnO_2: lithium ion insertion and manganese reduction according to the electrochemical equation

$$2\lambda\text{-}Mn^{4+}O_2 + Li^+ + 1e^- \rightarrow LiMn^{3+}Mn^{4+}O_4$$

The conductivity curve only accounts for electronic transport within the composite. Therefore, the electronic transport seems to be the limiting stage for manganese reduction, and hence, for lithium insertion in $LiMn_2O_4$.

Conclusions

Different composites have been prepared by cold pressing mixtures of $LiMn_2O_4$, CB, and PVDF. The microstructure of the composites shows that the $LiMn_2O_4$ particles are aggregated giving clusters whose size increase with raising the $LiMn_2O_4$ content. The CB particles are also aggregated in clusters.

The electrical conductivity of the composites depends on the relative distribution of $LiMn_2O_4$ and CB clusters according to a percolation process. Either $LiMn_2O_4$ or CB dominates the electrical conductivity of the composite depending on the kind of clusters that are connected along the composite. The discharge capacity of the composite when it is used as the cathode in a lithium cell seems also to depend on a percolation process. A sharp increase in capacity is observed for CB contents close to the percolation threshold deduced from the electrical conductivity. The good electronic transport due to the presence of connected CB clusters allows reduction of Mn^{4+} to Mn^{3+} and insertion of Li^+ in the electrode material. The current affects the kinetics of the electrochemical reaction in different ways depending on the microstructure of the composite. The effect is stronger for composites with CB contents close to the percolation threshold than for composites with higher CB contents.

Acknowledgments

Financial support through projects MAT 98-0904 (CICYT) and 07N/0059/1998 (CAM) is gratefully acknowledged. S.M. thanks the Spanish Ministry of Education and Culture for a grant.

Instituto de Ciencia de Materiales de Madid assisted in meeting the publication costs of this article.

References

1. G. Pistoia, *Lithium Batteries. New Materials, Developments, and Perspectives*, Elsevier, Amsterdam (1994).
2. M. Wakihara and O. Yamamoto, *Lithium Ion Batteries. Fundamentals and Performances*, Wiley-VCH, Tokyo (1998).
3. M. M. Thakeray, P. J. Johnson, L. A. De Picciotto, P. G. Bruce, and J. B. Goodenough, *Mater. Res. Bull.*, **19**, 179 (1984).
4. J. M. Tarascon, E. Wang, F. K. Shokooshi, W. R. McKinnon, and S. Colson, *J. Electrochem. Soc.*, **138**, 2859 (1991).
5. H. Huang and P. G. Bruce, *J. Electrochem. Soc.*, **141**, L106 (1994).
6. L. Chen, X. Huang, E. Kelder, and J. Schoonman, *Solid State Ionics*, **76**, 91 (1995).
7. C. Tsang and A. Manthiran, *Solid State Ionics*, **89**, 305 (1996).
8. P. Strobel, S. Rohs, and F. Le Cras, *J. Mater. Chem.*, **6**, 1591 (1996).
9. A. D. Robertson, S. H. Lu, W. F. Averill, and W. F. Howard, Jr., *J. Electrochem. Soc.*, **144**, 3500 (1997).
10. X. Qiu, X. Sun, W. Shen, and N. Chen, *Solid State Ionics*, **93**, 335 (1997).
11. P. Arora, B. N. Popov, and R. E. White, *J. Electrochem. Soc.*, **145**, 807 (1998).
12. M. Y. Song, D. S. Ahn, S. G. Kang, and S. H. Chang, *Solid State Ionics*, **111**, 237 (1998).
13. T. Le Mercier, J. Gaubicher, E. Bermejo, Y. Chabre, and M. Quarton, *J. Mater. Chem.*, **9**, 567 (1999).
14. N. V. Kosova, I. P. Asanov, E. T. Devyatkina, and E. G. Avvakumov, *J. Solid State Chem.*, **146**, 184 (1999).
15. G. X. Wang, D. H. Bradhurst, H. K. Liu, and S. X. Dou, *Solid State Ionics*, **120**, 95 (1999).
16. I. Balberg and S. Bozowski, *Solid State Commun.*, **44**, 551 (1982).
17. F. Carmona, P. Prudhon, and L. Barreau, *Solid State Commun.*, **51**, 255 (1984).
18. N. Deprez and D. S. McLachlan, *J. Phys D: Appl. Phys.*, **21**, 101 (1988).
19. M. A. J. Michels, Z. I. J. P. Brokken, W. M. Groenewoud, and A. Knoester, *Physica A*, **157**, 529 (1989).
20. A. Celzard, G. Furdin, J. F. Mareche, E. McRae, M. Dufort, and C. Deleuze, *Solid State Commun.*, **92**, 377 (1994).
21. M. B. Heaney, *Phys. Rev. B*, **52**, 12477 (1995).
22. L. Flandin, T. Prasse, R. Schueler, K. Schulte, W. Bauhofer, J. Y. Cavaille, *Phys. Rev. B*, **59**, 14349 (1999).
23. J. M. Amarilla, *Bol. Soc. Esp. Ceram. Vidrio*, **34**, 463 (1995).
24. V. Massarotti, D. Capsoni, M. Bini, G. Chiodelli, C. B. Azzoni, M. C. Mozzati, and M. Palleari, *J. Solid State Chem.*, **131**, 138 (1997).
25. Y. Shimakawa, T. Numata, and J. Tabuchi, *J. Solid State Chem.*, **131**, 138 (1997).
26. J. Sugiyama, T. Atsumi, A. Koiwai, and T. Sasaki, *J. Phys.: Condens. Matter*, **9**, 1729 (1997).
27. J. Molenda and W. Kucza, *Solid State Ionics*, **117**, 41 (1999).
28. H. Kawai, M. Nagata, H. Kageyama, H. Tukamoto, and A. R. West, *Electrochim. Acta*, **45**, 315 (1999).
29. J. R. Macdonald, *Impedance Spectroscopy. Emphasizing Solid Materials and Systems*, John Wiley & Sons, New York (1987).
30. J. T. S. Irvine, D. C. Sinclair, and A. R. West, *Adv. Mater.*, **2-3**, 132 (1990).
31. D. Stauffer and A. Aharony, *Introduction to the Percolation Theory*, Taylor and Francis, London (1994).
32. D. S. MacLachlan, M. Blaszkiewicz, and R. E. Newnham, *J. Am. Ceram. Soc.*, **73**, 2187 (1990).

Ningde Amperex Tech. Exhibit No. 2039
Zhuhai CosMX Battery Co. Ltd. v. Ningde Amperex Tech.
IPR2025-00431, U.S. Patent No. 11,799,131
Page 6 of 6